

Numerical investigation of the Rayleigh hypothesis for electromagnetic scattering by a particle

Baptiste Auguie¹, Walter R C Somerville^{1,2}, Stanley Roache¹ and Eric C Le Ru¹

¹The MacDiarmid Institute for Advanced Materials and Nanotechnology, School of Chemical and Physical Sciences, Victoria University of Wellington, PO Box 600, Wellington 6140, New Zealand

²Department of Physics and Mathematics, University of Hull, Kingston-upon-Hull HU6 7RX, UK

E-mail: baptiste.auguie@vuw.ac.nz

Received 7 March 2016, revised 5 April 2016

Accepted for publication 11 April 2016

Published 26 May 2016



CrossMark

Abstract

The validity of the Rayleigh hypothesis (RH) has been a long-standing issue in the applicability of the T -matrix method to near-field calculations, and despite numerous theoretical works, the practical consequences for numerical simulations have remained unclear. Such calculations are increasingly important in the field of nano-optics, for which accurate and efficient modeling tools are in high demand. We here tackle this challenge by investigating numerically the convergence behavior of series expansions of the electric field around spheroidal particles, which provides us with unambiguous examples to clarify the conditions of convergence. This study is made possible by the combination of alternative methods to compute near-fields accurately, and crucially, the recent improvements in the calculation of T -matrix elements free from numerical instabilities, as such errors would otherwise obfuscate the intrinsic convergence properties of the field series. The resulting numerical confirmation for the range of validity of the RH, complemented by a better understanding of the convergence behavior of the field expansions, is a crucial step toward future developments.

Keywords: T -matrix, near-field, Rayleigh hypothesis, multipoles

(Some figures may appear in colour only in the online journal)

1. Introduction

The T -matrix formulation, introduced by Waterman [1, 2], can be viewed as a generalization of Mie theory [3] to non-spherical particles. It is an elegant and powerful approach to describe electromagnetic scattering, where the incident and scattered electric fields are expanded as a series of multipoles such as

$$\mathbf{E}_{\text{sca}}(\mathbf{r}) = \sum_{n,m} p_{nm} \mathbf{M}_{nm}(k_1 \mathbf{r}) + q_{nm} \mathbf{N}_{nm}(k_1 \mathbf{r}), \quad (1)$$

where \mathbf{M}_{nm} and \mathbf{N}_{nm} are magnetic and electric multipole fields, and form a complete basis for the solution of the Helmholtz equation obtained via separation of variables in spherical coordinates [3–5]. The coefficients of the series expansion for the scattered field depend linearly on those of

the incident field, and this relation defines the so-called T -matrix [5]. Knowledge of the T -matrix provides in theory the complete solution of the scattering problem at a specific wavelength, for any incident field. The T -matrix method has been extensively studied and successfully applied to compute the scattering properties of particles of various shapes in a wide variety of contexts, ranging from astrophysical and atmospheric studies to nano-optics [6].

However, the applicability of the T -matrix approach to near-field calculations remains somewhat questionable, and certainly less well-understood than for far-fields. Many fewer studies have considered this aspect [7–10], and misconceptions still persist in the literature. With an ever-growing interest in nano-optics and plasmonics in particular, the demand for fast and accurate light scattering calculations in close proximity to

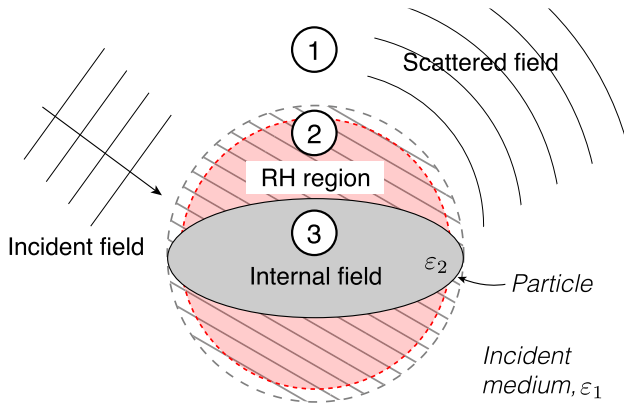


Figure 1. Schematic description of the scattering problem. A scatterer embedded in a non-absorbing medium (with relative dielectric functions ϵ_2 and ϵ_1 , respectively) is excited by an incident field, e.g a plane wave, at a free-space wavelength λ . Three regions of space may be distinguished. (1) Outside a circumscribing sphere, the total (incident + scattered) field is rigorously expanded in a series of multipole fields as in equation (1). (2) (‘Rayleigh hypothesis region’) Within the circumscribing sphere, but outside the particle, the RH assumes that an expansion of the form of equation (1) is valid, which is not always true. For spheroids, we will indeed show that this is only true outside the focal circle (dashed red circle). Region (3) is the interior of the particle, where the internal field can be described as a convergent series of regular multipoles as in equation (2).

nanostructures is setting new challenges for computational tools. In the context of the T -matrix, its numerical accuracy in near-field studies is often linked to a long-standing issue known as the Rayleigh hypothesis (RH) [5, 11–16], the validity of which is known to be limited. In essence, the RH postulates that the series expansion for the scattered field (outside the particle) remains valid everywhere outside the particle, including arbitrarily close to the particle surface. In standard derivations of the T -matrix theory, however, it is only proved to be valid outside the circumscribing sphere (see figure 1). The intermediate region, inside the circumscribing sphere but exterior to the particle, is the subject of this work: can we use the series expansion for the scattered field to compute the near-field everywhere in this region?

It could be argued that the validity of the RH for electromagnetic scattering was fully investigated theoretically and settled 40 years ago [14, 15], yet one of the reasons why it is still much debated today is that those mathematical considerations do not easily translate to practical computations, where numerical instabilities/errors prevent reliable numerical investigations. This was in fact recently highlighted in the case of diffraction by a grating [17], the context in which the RH was originally formulated [18, 19]. As noted in several reviews and monographs [5, 16, 20, 21], there is still considerable uncertainty regarding the exact range of validity of the RH, and whether it affects the applicability of the T -matrix method for accurate near-field computations. The main obstacle to detailed investigations into the RH is arguably due to the numerical difficulties in obtaining an accurate T -matrix, and therefore accurate expansion coefficients, for relatively large multipole orders.

The extended boundary-condition method (EBCM), also known as the null-field method, is a standard method to compute the T -matrix of a scatterer, with close connections to the analytical Mie solution for spherical particles; for the general case of non-spherical particles, the T -matrix elements are obtained by solving a linear system involving many surface integrals on the particle surface [1, 2, 5, 16, 22–25]. This approach, sometimes simply called the T -matrix method or formalism, was developed in the 1960–70s [2, 22, 26] and remains one of the most efficient techniques for the study of electromagnetic scattering, particularly by axisymmetric particles, for which the formulas and computational efforts simplify considerably.

Despite its performance and almost analytical rooting, the EBCM suffers from numerical instabilities for large multipole order and/or elongated particles. Recently, we have identified the origin of those problems in the special case of spheroids [27] and proposed an improved algorithm to overcome them [28]. This new implementation, for which user-friendly codes are freely available [29], provides unprecedented accuracy for the computation of the T -matrix and the field expansion coefficients [30]. It therefore provides a reliable basis, enabling us to study the range of validity of the RH in the context of near-field computations without the interference of numerical instabilities.

To this end, we first describe and test a general method to accurately compute the near fields within the T -matrix framework. Those results are then used as benchmark to study the convergence of field expansions in the RH region, thus providing a rigorous numerical confirmation of its region of validity. Explicit illustrations of the failure of the RH and of the consequences in near-field calculations are readily apparent in such example calculations. Although our results will be based on specific examples and thus not fully general in a strict mathematical sense, this numerical study provides a much clearer and practical picture of the validity of the T -matrix method and associated field expansions. Our approach also provides further information, as it allows us to study the convergence properties of the field expansions, an important information for any numerical application of the method. We hope this discussion will help clarify some of the contradictions found in the literature and provide a solid base from which to explore further these issues numerically, or from a more rigorous and general perspective.

2. Computing accurate near-fields

Within the T -matrix/EBCM framework, the internal field (inside the scatterer) is also written as a series expansion, which for physical reasons involves regular vector spherical wavefunctions RgM and RgN [5], explicitly:

$$\mathbf{E}(\mathbf{r}) = E_0 \sum_{n,m} c_{nm} \text{RgM}_{nm}(k_2 \mathbf{r}) + d_{nm} \text{RgN}_{nm}(k_2 \mathbf{r}), \quad (2)$$

where the expansion coefficients c_{nm} and d_{nm} of the internal fields are calculated using the EBCM in a similar fashion as those of the scattered field [5, 31], and $k_2 = 2\pi\sqrt{\epsilon_2}/\lambda$ is the

wave vector inside the particle. It is generally accepted that this internal field expansion is valid everywhere inside the scatterer [2, 5, 7, 8] and in particular on the internal side of its surface. Recent works [32] however suggest that this is only true for convex particles and that the entire T -matrix/EBCM framework may fail for some types of non-convex scatterers. We avoid this issue here by restricting our discussion to convex scatterers (spheroids) and to the RH for the scattered (external) field.

To circumvent the RH, three general approaches have so far been proposed to compute near-fields in the RH region. The first one consists in calculating the field exactly on the surface [7–10, 29], as computed from the field expansion of the internal field (equation (2)). Standard boundary conditions can then be applied to obtain the surface field immediately outside the particle. This approach yields accurate results, but is obviously limited to the particle surface only. To obtain the near-field elsewhere in the RH region, a second approach has been proposed [33, 34] based on a scattered field expansion in terms of *both* irregular and regular multipolar fields. Point matching techniques are used to find the coefficients of this alternative expansion in the region of interest, from a knowledge of the fields on the boundaries of this region. The accuracy and numerical convergence of this method has not been studied and assessed in detail.

We will here use an alternative exact approach introduced in [33] and based on the standard surface-integral formulation of the EM scattering problem. Within this framework, the scattered field can be written as the following surface integral (equation 5.168 in [5]), also known as Stratton–Chu formula

$$\mathbf{E}_{\text{sca}}(\mathbf{r}) = \int_S dS \left\{ i\omega\mu_0 [\mathbf{n} \times \mathbf{H}(\mathbf{r}')] \cdot \overleftrightarrow{G}(\mathbf{r}', \mathbf{r}) + [\mathbf{n} \times \mathbf{E}(\mathbf{r}')] \cdot [\nabla \times \overleftrightarrow{G}(\mathbf{r}', \mathbf{r})] \right\}, \quad (3)$$

where \overleftrightarrow{G} is the dyadic Green’s function. This formula expresses the scattered field in terms of the tangential electric and magnetic fields on the particle surface, or equivalently and more physically, as the field created by induced electric ($\mathbf{p} = \mathbf{n} \times \mathbf{H}$) and magnetic ($\mathbf{m} = \mathbf{n} \times \mathbf{E}$) dipoles. This is rewritten for convenience as

$$\mathbf{E}_{\text{sca}}(\mathbf{r}) = E_0 \int_S dS \left\{ k_2 \left[\mathbf{n} \times \frac{\mathbf{H}(\mathbf{r}')}{H_0} \right] \cdot \overleftrightarrow{G}(\mathbf{r}', \mathbf{r}) + \left[\mathbf{n} \times \frac{\mathbf{E}(\mathbf{r}')}{E_0} \right] \cdot [\nabla \times \overleftrightarrow{G}(\mathbf{r}', \mathbf{r})] \right\}, \quad (4)$$

where $H_0 = k_2 E_0 / (i\omega\mu_0)$. The surface fields are obtained from the series expansions of the internal field, i.e. equation (2) for the electric field and

$$\mathbf{H}(\mathbf{r}) = H_0 \sum_{n,m} d_{nm} \text{RgM}_{nm}(k_2 \mathbf{r}) + c_{nm} \text{RgN}_{nm}(k_2 \mathbf{r}) \quad (5)$$

for the magnetic field [5].

The dyadic Green’s function in the embedding medium has the standard form [5]:

$$\overleftrightarrow{G}(\mathbf{r}', \mathbf{r}) = \left(\overleftrightarrow{I} + \frac{1}{k_1^2} \nabla \otimes \nabla \right) \frac{\exp(ik_1|\mathbf{r}' - \mathbf{r}|)}{4\pi|\mathbf{r}' - \mathbf{r}|} \quad (6)$$

with $k_1 = 2\pi\sqrt{\epsilon_1}/\lambda$ the wave vector in the surrounding medium. Using the shorthand notations $\mathbf{R} = \mathbf{r}' - \mathbf{r}$, $R = |\mathbf{R}|$, and $\mathbf{e}_R = \mathbf{R}/R$, explicit expressions for the terms appearing in equation (4) read as:

$$\mathbf{p} \cdot \overleftrightarrow{G}(\mathbf{r}', \mathbf{r}) = \frac{e^{ik_1 R}}{4\pi R} \left\{ [\mathbf{p} - (\mathbf{e}_R \cdot \mathbf{p})\mathbf{e}_R] + [3(\mathbf{e}_R \cdot \mathbf{p})\mathbf{e}_R - \mathbf{p}] \left(\frac{1}{(k_1 R)^2} - \frac{i}{k_1 R} \right) \right\}, \quad (7)$$

$$\mathbf{m} \cdot [\nabla \times \overleftrightarrow{G}(\mathbf{r}', \mathbf{r})] = ik_1 \frac{e^{ik_1 R}}{4\pi R} [\mathbf{e}_R \times \mathbf{m}] \left(1 - \frac{1}{ik_1 R} \right). \quad (8)$$

Equations (4)–(8) were used to compute the scattered field in the near-field region. In practice, the surface integral in equation (4) is carried out using a Gaussian quadrature over both θ and ϕ , and we used for convenience the same quadrature order N_q for both (therefore giving N_q^2 quadrature points for the surface integral). This method of calculating the near-field is also implemented in our freely-available codes [29].

By combining this surface-integral approach with the improved T -matrix formulation for spheroids, high accuracy in the near-field region can be achieved reliably. To illustrate this, we consider an example relevant to plasmonics, where near-fields are crucial, namely an elongated silver nanoparticle modeled as a prolate spheroid of semi-axes 40×20 nm (aspect ratio of 2) embedded in water. Using the accurate T -matrix/ EBCM implementation discussed previously [28–30], we can calculate most relevant properties efficiently and accurately, as illustrated in figures 2(a) and (b). The maximum relative error obtained for the predicted far-field and surface-field data shown in figures 2(a) and (b) is 10^{-14} (as estimated by changing the multipole order and number of quadrature points [29]), attesting to the extreme accuracy of the method. Those surface fields are then used in equation (4) to calculate the near-field in the vicinity of the particle, including in the RH region. Those are compared to a fully numerical solution of the same problem using state-of-the-art surface-integral equation (SIE) methods [35]. The results of this comparison, shown in figure 2(c), readily demonstrate that equation (4) provides accurate near-fields, including in the RH region, although it progressively fails when approaching the particle too closely (below 1 nm in this example). This inaccuracy is expected since the Green’s function becomes large and ultimately singular as the observation point approaches the surface. In order to compensate for this approaching singularity, more integration points are needed in the numerical calculation of the integral, as shown in figures 2(c) and (d). Note that the SIE solution is arguably one of the best fully numerical tools to solve this problem [35], yet despite the finesse of the mesh (which is close to the limits of what is currently tractable

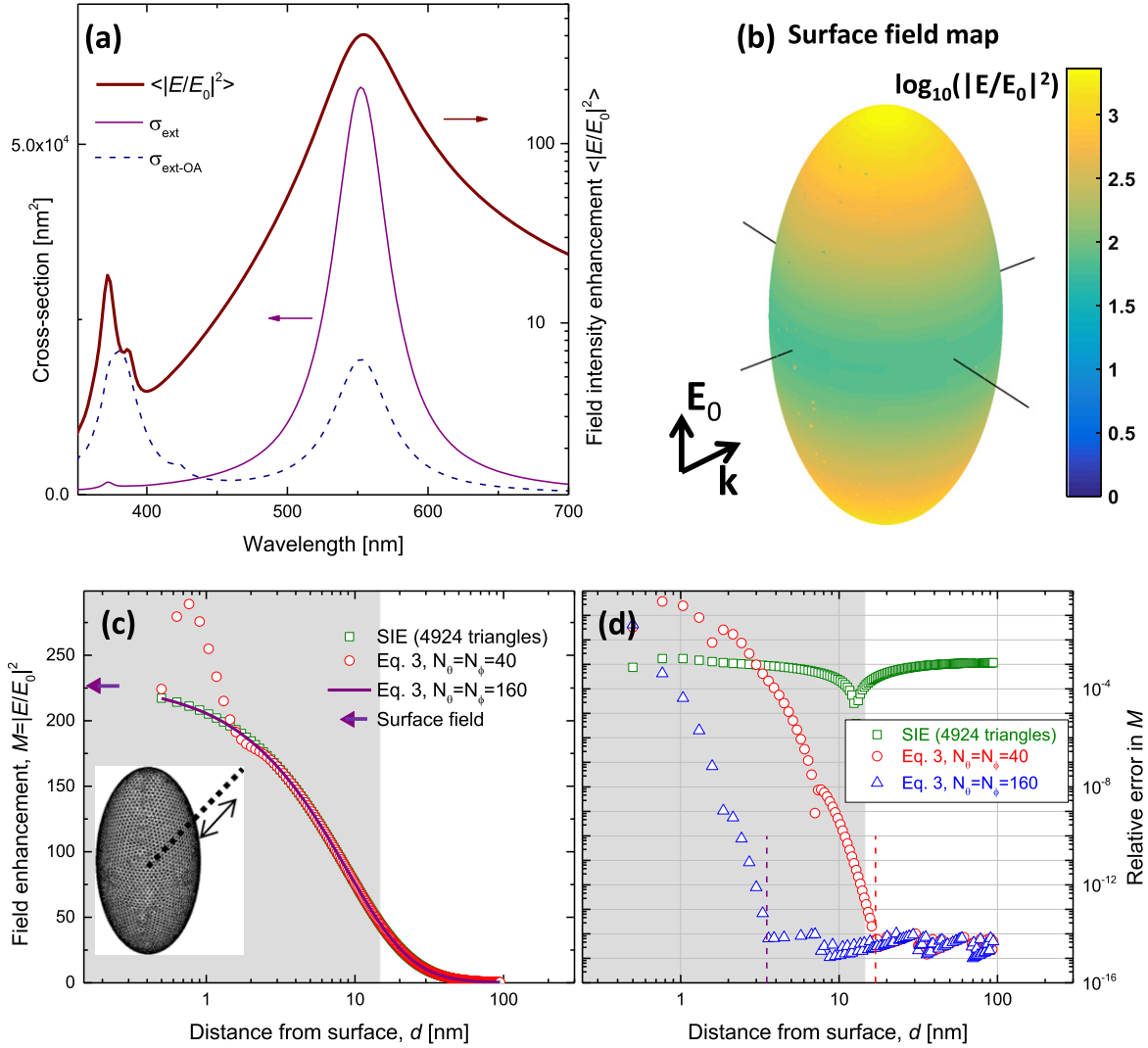


Figure 2. Example of near-field computations using the integral formulation of equation (4) for a silver prolate spheroid of semi-axes 40×20 nm (aspect ratio of 2) in water (refractive index 1.33). The T -matrix is calculated up to multipole order $N = 20$ using 40 Gauss–Legendre nodes for the integrals. In (a) and (b) the field enhancement factor on the surface $M = |E/E_0|^2$ is calculated from the internal field expansions for incident excitation polarized along the long axis. The predicted spectral dependence of the extinction cross-section and the surface-averaged $\langle M \rangle$ are shown in (a), along with the orientation-averaged extinction cross-section. The peaks at 552 nm correspond to the main plasmon resonance of this metallic nanoparticle. The surface-field distribution at resonance ($\lambda = 552$ nm, where the relative refractive index is $s = 0.0556 + 2.53i$) is shown in (b). (c) Near-field intensity of the scattered field calculated at a distance d along the $x = z, y = 0$ line, either using a fully-numerical surface-integral equation solution with the mesh shown in the inset, or using equation (4) with 40^2 and 160^2 integration points. The surface field ($d = 0$) obtained from (b) is shown as a purple arrow. (d) Relative error in the computation of the near-field. The T -matrix results of equation (4) with 1280^2 integration points were also calculated and taken as reference for error calculations. The shaded area in (c) and (d) corresponds to the RH region (inside the circumscribing circle).

on a standard personal computer), a relative accuracy of 1% only is achieved for the near-fields. In contrast, almost-perfect (within double precision) $\sim 10^{-14}$ precision is obtained with the T -matrix method. Moreover, the T -matrix solution is about 600 times faster than the SIE. With $N_q^2 = (160)^2$ integration points, this high-precision is achieved down to ~ 3 nm away from the surface, and a precision better than 1% remains down to $d = 0.5$ nm. Since the surface-field ($d = 0$) is easily obtained from the internal field, these results should be sufficient for the vast majority of applications, and smooth interpolation may be used if sub-nanometer distances are of interest, such as in surface-enhanced Raman scattering [36]. We note that a more optimized implementation of this approach could be developed

using an adaptive numerical quadrature, which would efficiently cope with the Green’s function singularity for small d by increasing the number of quadrature points around the singularity only. Alternatively, singularity-suppression techniques may be applied to further improve the accuracy of integration [37].

In the context of light scattering by spheroidal particles, we mention the existence of analytical solutions obtained by Asano and Yamamoto [38] and Farafonov [39] based on the separation of variables method in spheroidal coordinates. This method can also provide accurate results, and could be used as an alternative benchmark for comparison, but the T -matrix/EBCM method has been the subject of many more

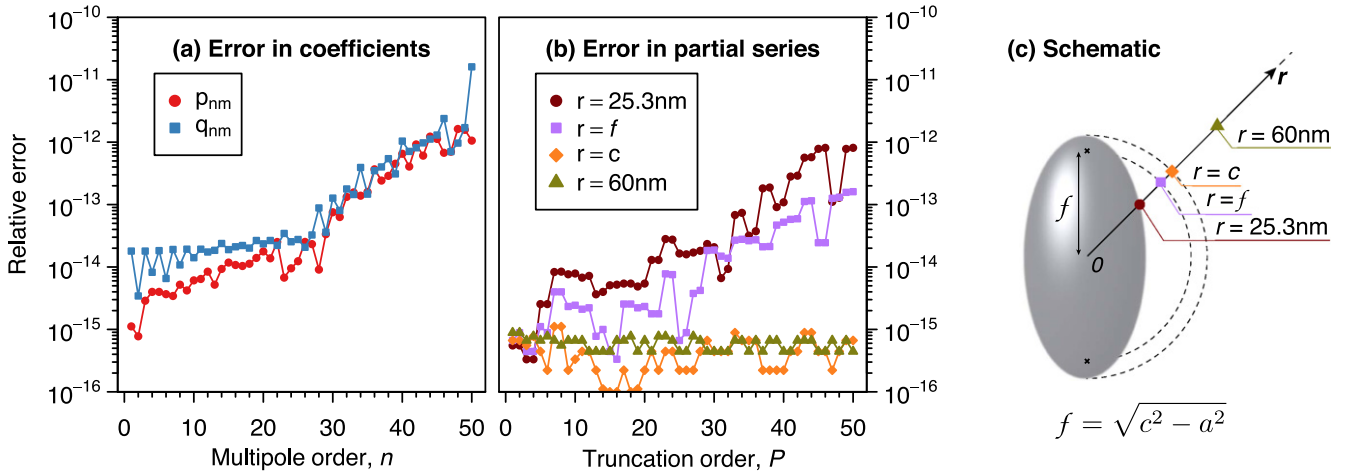


Figure 3. (a) Relative error in the computed scattered field expansion coefficients, p_{nm} and q_{nm} as a function of multipole order n for the same example as in figure 2, i.e. a 40×20 nm silver prolate spheroid in water at 552 nm. The error is computed for all $|m| \leq n$ and the maximum error is retained. (b) Relative error in the partial series (summed up to multipole order P) of the scattered field, see equation (9), at selected points along the $x = z, y = 0$ line. In both cases, the T -matrix computations are first carried out up to maximum multipole order $N = 55$, with 100 quadrature points. The relative error is then estimated by comparing the results to those obtained with $N = 85$ and 135 quadrature points. (c) Schematic showing the location of the points where the convergence is studied on the $x = z, y = 0$ line. The semi-axes are here $a = 20$ nm and $c = 40$ nm, so the surface corresponds to $r \approx 25.3$ nm and the focal distance from the origin is $f \approx 34.6$ nm.

studies and its numerical stability and convergence is better established than for spheroidal wave functions. We therefore consider the converged T -matrix results as our reference, with independent confirmation of their validity provided by the SIE method.

3. Numerical verification of the RH

The remarkable stability of the new T -matrix implementation also allows the accurate calculation of the field expansion coefficients up to large multipole orders, as illustrated in figure 3(a). It is clear that the scattered field expansion coefficients (p_{nm} and q_{nm} , see equation (1)) can be computed to a relatively high accuracy ($\sim 10^{-12}$) up to large multipole orders (at least $n = 50$ in the example of figure 3). As a consequence, as shown in figure 3(b), a similar accuracy of better than $\sim 10^{-12}$ is also obtained for the corresponding partial series $\mathbf{E}_P(\mathbf{r})$, i.e. the sum in equation (1) truncated at a maximum multipole order P :

$$\mathbf{E}_P(\mathbf{r}) = \sum_{\substack{n=1 \\ |m| \leq n}}^{n=P} p_{nm} \mathbf{M}_{nm}(k_1 r) + q_{nm} \mathbf{N}_{nm}(k_1 r) \equiv \sum_{n=1}^P \mathbf{E}_n(\mathbf{r}). \tag{9}$$

This therefore opens the way for a detailed numerical investigation into the validity of the RH. The principle of the approach is simple: the partial series $\mathbf{E}_P(\mathbf{r})$ for the scattered field in the near-field region are calculated to a high accuracy and their convergence is tested in comparison to the correct high-precision result obtained using the independent method validated in the previous section. Such a study is summarized in figure 4 for the same example as already considered. Those numerical results (supplemented by many similar tests on

different spheroidal geometries) suggest that the convergence properties depend on the position with respect to the sphere centered at the origin and going through the two spheroid focal points, i.e. $r = f$ where $2f$ is the interfocal distance. The scattered field expansions are only convergent for $r > f$, where they converge towards the correct results. The convergence can be quite slow for r close to f , but as we move further away, a relative accuracy of 10^{-15} can be obtained provided enough multipoles are included. In contrast, the series expansion appear to diverge for $r < f$. Note that this divergence cannot here be attributed to numerical instabilities, since as we showed in figure 3, those partial series are very accurate. They simply reflect the fact that those series are divergent and cannot be used to evaluate the scattered field. At the boundary between those two regimes, the partial series show an oscillatory behavior, from which we cannot infer its ultimate divergence/convergence. Similar conclusions are obtained, perhaps more visually, when considering the maps of the error in the fields computed from the series expansions, as illustrated in figure 5.

4. Origin of convergence/divergence

These numerical investigations also allow us to better understand the cause of the series divergence in regions where the RH fails. The convergence properties of these series can conveniently be studied by the standard ratio test, explicitly:

$$\sum_n a_n \text{ converges} \iff \lim_{n \rightarrow \infty} \frac{|a_{n+1}|}{|a_n|} < 1, \tag{10}$$

$$\sum_n a_n \text{ diverges} \iff \lim_{n \rightarrow \infty} \frac{|a_{n+1}|}{|a_n|} > 1 \tag{11}$$

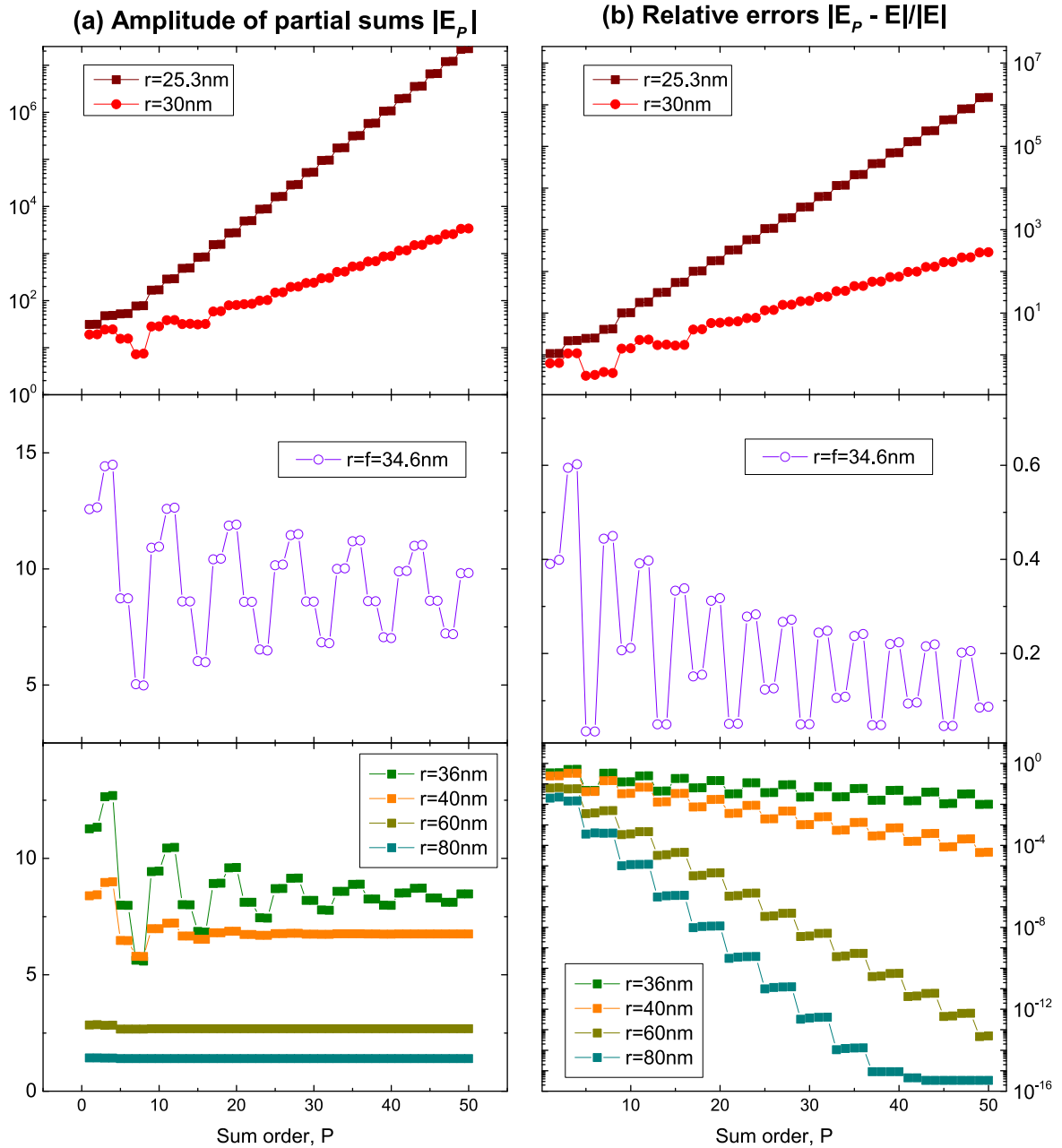


Figure 4. The convergence of the partial series expansions for the scattered field is studied by considering the truncation order (P) dependence of both (a) the amplitude $|E_p|$, and (b) the relative error $|E_p - E_{ex}|/|E_{ex}|$ with respect to the exact result E_{ex} obtained from equation (4) with 160^2 integration points. Those are calculated for the same example as in figure 2 along a line defined by $\theta = \pi/4$ and $\phi = 0$. Different positions are considered by comparing r with the distance of the spheroid foci from the origin, i.e. $f = \sqrt{c^2 - a^2} \approx 34.6$ nm in this example. Clear divergence is observed for $r < f$ (top), while convergence is obtained for $r > f$ (bottom), albeit slowly when r is close to f . An oscillatory behavior is obtained for $r = f$ (middle).

and we therefore need to understand the asymptotic behavior (for large n) of the terms in our expansions, i.e. $E_n(\mathbf{r})$ in equation (9). In the example considered so-far, the terms corresponding to $m = 0$ and to the electric multipoles N_{nm} are dominant and we therefore focus on those for simplicity, but the conclusions naturally extend to the general case. In this case, the terms in the scattered field expansion can be approximated as $|E_n(\mathbf{r})| \approx |q_{n0} N_{n0}(k_1 \mathbf{r})|$. The asymptotic

expression of the multipole field for large n is [40]:

$$|N_{n0}(k_1 \mathbf{r})| \sim \frac{(2n - 1)!!}{(k_1 r)^{n+2}} f_n(\theta, \phi), \quad (12)$$

where !! refers to the double factorial and the exact expression for $f_n(\theta, \phi)$ will be irrelevant, except for the fact that for large n

$$\frac{f_{n+1}(\theta, \phi)}{f_n(\theta, \phi)} \rightarrow 1. \quad (13)$$

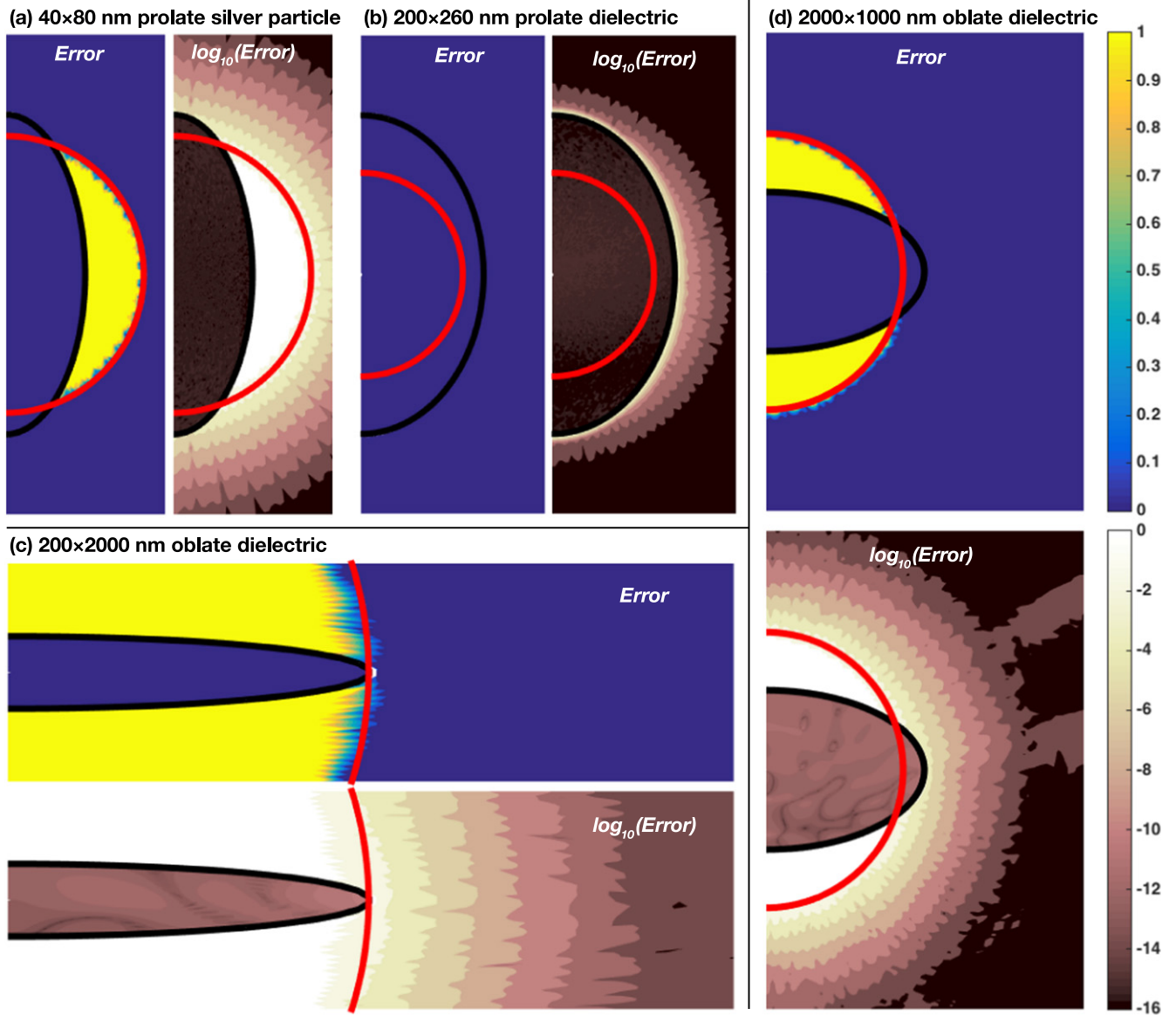


Figure 5. Maps of the relative errors (capped at a maximum of 1 for clarity) in the fields computed from the series expansion, shown both on linear and \log_{10} scales. The relative error in the scattered field expansion (compared to the result of equation (4) with 160^2 quadrature points) is shown outside the particle. The relative error in the internal field expansion (as compared with the same expansion with 25 extra multipolar orders) is shown inside the particle. The particle surface is shown as a black line, while the red line corresponds to the sphere $r = f$ delimiting the region of validity of the RH for spheroids. Four representative cases are presented: (a) a silver prolate spheroid of axes 40×80 nm in water excited at its plasmon resonance at 552 nm along its long axis (k_x, E_z). (b) A low aspect-ratio ($h = 1.3$) low-absorbing ($n = 1.5 + 0.02i$) prolate spheroid in air excited at 552 nm along its short axis (k_z, E_x). (c) A high aspect-ratio ($h = 10$) low-absorbing ($n = 1.5 + 0.02i$) oblate spheroid in air excited at 552 nm along its long axis (k_z, E_x). (d) A large non-absorbing dielectric ($n = 1.5$) oblate spheroid of axes $2 \times 1 \mu\text{m}$ in air excited at 552 nm along its long axis (k_x, E_z).

This leads us to introduce normalized expansion coefficients as follows:

$$\tilde{q}_{n0} = (2n - 1)!! q_{n0}. \tag{14}$$

Thanks to the expressions above, the convergence study can be reduced to studying the asymptotic behavior of \tilde{q}_{n0} , and in

particular of the ratio:

$$Q(r) = \lim_{n \rightarrow \infty} \frac{1}{(k_1 r)^2} \frac{|\tilde{q}_{n+2,0}|}{|\tilde{q}_{n,0}|} \tag{15}$$

(note that for spheroids $q_{n0} = 0$ if n is even, and the ratio test is carried out on consecutive non-zero terms). If $Q(r) < 1$, the series converges approximately like a geometric series of

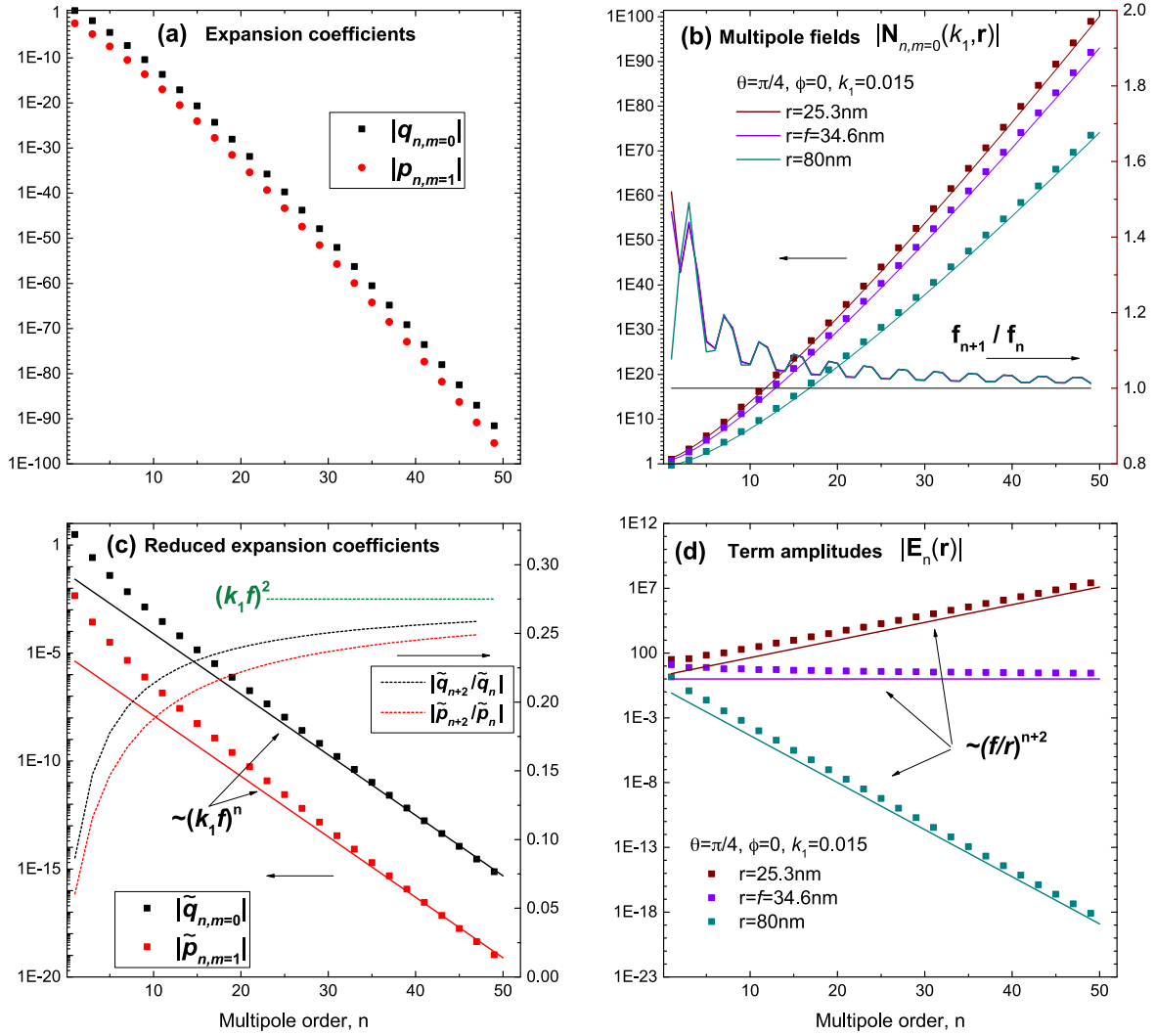


Figure 6. Convergence and approximations of the terms in the series expansions for the same example as in figure 3. (a) n -dependence of the amplitude of the dominant scattered field expansion coefficients $|q_{n,m=0}|$. Other coefficients exhibit similar behavior as shown here for $|p_{n,m=1}|$. Note that those coefficients are zero for even n for spheroids under plane wave excitation. (b) Approximation of the electric multipole field: the computed amplitude $|N_{n,m=0}(k_1, \mathbf{r})|$ is shown for three positions (symbols) along with their approximation as $(2n - 1)!! / (k_1 r)^{n+2}$ (solid lines). We also compute in each case the ratio $f_n = |N_{n,m=0}(k_1, \mathbf{r})| (k_1 r)^{n+2} / (2n - 1)!!$ and show the convergence of f_{n+1} / f_n (dashed lines). (c) Reduced expansion coefficients (equation (14)), $|\tilde{q}_{n,m=0}|$ and $|\tilde{p}_{n,m=1}|$ (symbols) along with their postulated asymptotic form as $A (k_1 f)^n$ (solid lines). The asymptotic geometric-like nature of those coefficients is also evident in the convergence of the ratio of consecutive terms (dashed lines). (d) n -dependence of the amplitude of each term in the scattered field series, $|E_n(\mathbf{r})|$ (symbols), along with their geometric approximation (lines).

common ratio $\sqrt{Q(r)}$, while if $Q(r) > 1$, it diverges like the corresponding geometric series. For $Q(r) = 1$, the series may diverge or converge but in the latter case the convergence is slower than geometric.

With these definitions, the series convergence can again be investigated numerically as illustrated in figure 6. The n -dependence for the expansion coefficients q_{n0} (which are independent of \mathbf{r}) is shown in (a) and the asymptotic form of $|N_{n0}(k_1 \mathbf{r})|$ is compared to the exact result in (b). In (c), we study the convergence of $\frac{\tilde{q}_{n+2,0}}{\tilde{q}_{n,0}}$, which suggests (along with

similar studies for different spheroidal geometries) that

$$\lim_{n \rightarrow \infty} \frac{|\tilde{q}_{n+2,0}|}{|\tilde{q}_{n,0}|} = (k_1 f)^2, \Rightarrow Q(r) = \left(\frac{f}{r}\right)^2, \quad (16)$$

where f is the focal distance from the origin. We then easily deduce from the ratio test that the series converge for $r > f$ and diverge for $r < f$ and that the ‘speed’ of this convergence/divergence is directly related to the ratio f/r , i.e. it behaves like the geometric series of common ratio f/r as shown explicitly in figure 6(d). The convergence/divergence regions of the field

expansions and the validity of the RH therefore appear as a natural consequence of the asymptotic properties of the expansion coefficients. These considerations moreover provide a simple practical criterion for when those expansions should be used in numerical computations. For example, if $f/r = 0.95$, although convergent, the expansion should not be used in practical calculations as almost 100 multipole orders will be needed for an accuracy of the order 1%. Alternative methods discussed earlier should therefore be preferred.

5. Discussion and conclusion

These results should not be surprising in view of earlier studies [14, 15], which were very recently reinforced for a similar framework [32] corresponding to the low-frequency limit (electrostatic approximation) of the standard T -matrix method. We can summarize those conclusions as follows:

- As illustrated here, the RH for the scattered field is neither always valid nor always invalid as this will depend on the scatterer shape (and this is true not only for spheroids, but also for any smooth convex shapes).
- Even when the RH is not valid all the way down to the surface of the scatterer, the T -matrix method remains valid (for convex particles) and the scattered field expansion remains valid where it converges.
- For convex and sufficiently smooth scatterers, the range of validity of the RH is outside a sphere centered at the origin and containing all the singularities of the analytic continuation of the field expansion. Finding the location of those singularities *a priori* is not straightforward, but in the special case of spheroidal particles, they are located at the foci of the ellipse defining the particle [14, 41]. For spheroids, the RH is therefore valid inside part of the circumscribing sphere, down to the sphere intersecting the foci ($r = f$), inside which it then fails. As a consequence, for spheroidal scatterers the RH is valid all the way down to the surface only when the aspect ratio (long axis divided by short axis) is smaller than $\sqrt{2}$. All these points were vividly illustrated and confirmed by our numerical investigations (see figure 5 for example).
- We have also clearly highlighted the reasons behind the failure of the RH: the series expansions are valid everywhere in their region of convergence and the RH fails in the regions where those series become divergent. This interpretation then supports the argument that the analytic continuation of the scattered field expansion is in general a valid mathematical description of the scattered field all the way down to the surface. The RH would therefore be valid everywhere when interpreted in the wider sense of analytic continuation of series [14, 15].

In practice, computing explicitly the analytic continuation of such series is challenging. Our proposed and demonstrated method of calculating the near-field should

therefore be preferred in regions where the RH fails ($r < f$ for spheroids) and even when approaching this region ($r \gtrsim f$) to avoid issues with slowly-convergent series.

We hope that this study will help clarify the understanding of the RH in the context of electromagnetic scattering by particles, and lead to improvements and a wider dissemination of near-field calculations using the T -matrix/EBCM framework.

Funding information

Rutherford Discovery Fellowship (Royal Society of New Zealand).

References

- [1] Waterman P C 1969 *J. Opt. Soc. Am.* A **45** 1417–29
- [2] Waterman P C 1971 *Phys. Rev. D* **3** 825–39
- [3] Bohren C F and Huffman D R 1983 *Absorption and Scattering of Light by Small Particles* (New York: Wiley)
- [4] Morse P and Feshbach H 1953 *Methods of Theoretical Physics* (New York: McGraw-Hill)
- [5] Mishchenko M I, Travis L D and Lacis A A 2002 *Scattering, Absorption and Emission of Light by Small Particles* 3rd edn (Cambridge: Cambridge University Press)
- [6] Mishchenko M I, Zakharova N T, Khlebtsov N G, Wriedt T and Videen G 2014 *J. Quant. Spectrosc. Rad. Transfer* **146** 349–54
- [7] Barber P, Chang R and Massoudi H 1983 *Phys. Rev. Lett.* **50** 997–1000
- [8] Barber P W, Chang R K and Massoudi H 1983 *Phys. Rev. B* **27** 7251–61
- [9] Cline M, Barber P and Chang R 1986 *J. Opt. Soc. Am. B* **3** 15–21
- [10] Boyack R and Le Ru E C 2009 *Phys. Chem. Chem. Phys.* **11** 7398–405
- [11] Burrows M 1969 *Electron. Lett.* **5** 277–8
- [12] Bates R 1969 *Electron. Lett.* **5** 654–5
- [13] Burrows M 1969 *Electron. Lett.* **5** 694–5
- [14] Millar R 1969 *Electron. Lett.* **5** 416–7
- [15] Bates R 1975 *IEEE Trans. Microw. Theory Tech.* **23** 605–23
- [16] Rother T and Kahnert M 2009 *Electromagnetic Wave Scattering on Nonspherical Particles* (Berlin: Springer)
- [17] Tishchenko A V 2009 *Opt. Express* **17** 17102–17
- [18] Lord Rayleigh 1907 *Proc. R. Soc. A* **79** 399–416
- [19] Millar R F 1971 *Math. Proc. Camb. Phil. Soc.* **69** 217–25
- [20] Kahnert F M 2003 *J. Quant. Spectrosc. Rad. Transfer* **79–80** 775–824
- [21] Farafonov V G and Il'in V B 2006 *Single Light Scattering: Computational Methods* (Berlin: Springer-Verlag) pp 127–77
- [22] Barber P and Yeh C 1975 *Appl. Opt.* **14** 2864–72
- [23] Waterman P C 1979 *J. Appl. Phys.* **50** 4550
- [24] Barber P W and Hill S C 1990 *Light Scattering by Particles: Computational Methods* (Singapore: World Scientific)
- [25] Doicu A, Wriedt T and Eremin Y A 2006 *Light Scattering by Systems of Particles: Null-Field Method with Discrete Sources: Theory and Programs (Springer Series in Optical Sciences vol 124)* (Berlin: Springer)
- [26] Waterman P C 1965 *Proc. IEEE* **53** 805–12
- [27] Somerville W R C, Auguie B and Le Ru E C 2012 *J. Quant. Spectrosc. Rad. Transfer* **113** 524–535

- [28] Somerville W R C, Augu   B and Le Ru E C 2013 *J. Quant. Spectrosc. Rad. Transfer* **123** 153–68
- [29] Somerville W R C, Augu   B and Le Ru E C 2016 *J. Quant. Spectrosc. Rad. Transfer* **174** 39–55
- [30] Somerville W R C, Augu   B and Le Ru E C 2015 *J. Quant. Spectrosc. Rad. Transfer* **160** 29–35
- [31] Somerville W R C, Augu   B and Le Ru E C 2011 *Opt. Lett.* **36** 3482–4
- [32] Farafonov V G and Ustimov V I 2015 *Opt. Spectrosc.* **119** 1022–33
- [33] Doicu A and Wriedt T 2010 *J. Quant. Spectrosc. Rad. Transfer* **111** 466–73
- [34] Forestiere C, Iadarola G, Dal Negro L and Miano G 2011 *J. Quant. Spectrosc. Rad. Transfer* **112** 2384–94
- [35] Raziman T V, Somerville W R C, Martin O J F and Le Ru E C 2015 *J. Opt. Soc. Am. B* **32** 485–92
- [36] Le Ru E C and Etchegoin P G 2009 *Principles of Surface Enhanced Raman Spectroscopy and Related Plasmonic Effects* (Amsterdam: Elsevier)
- [37] Reid M, White J and Johnson S 2015 *IEEE Trans. Antennas Propag.* **63** 195–209
- [38] Asano S and Yamamoto G 1975 *Appl. Opt.* **14** 29–49
- [39] Voshchinnikov N and Farafonov V 1993 *Astrophys. Space Sci.* **204** 19–86
- [40] Le Ru E C, Somerville W R C and Augu   B 2013 *Phys. Rev. A* **87** 012504
- [41] Maystre D and Cadilhac M 1985 *J. Math. Phys* **26** 2201–4